Local high-slope effects on sediment transport and fluvial bed-form dynamics

Local high-slope effects on sediment transport and fluvial bed form dynamics

Simona Francalanci,[1] Luca Solari,[2] and Marco Toffolon[3]

Received 17 July 2008; revised 29 December 2008; accepted 27 January 2009; published 28 May 2009.

[1] We investigate the morphodynamic evolution of an arbitrarily tilted, coarse, mobile bed under the action of a free surface water flow. The analysis is based on the experimental observations of the evolution of a mobile bed from its initial, laterally tilted configuration to the final laterally flat state, due to the presence of a lateral component of bed load transport. Measurements of the bed topography at different times allow one to reconstruct the flattening process. The experimental observations are interpreted by means of a three-dimensional numerical hydromorphodynamic model employing different relationships, linear and nonlinear, to evaluate bed load intensity and direction. The analysis shows that the inclusion of nonlinear gravitational effects in the description of the bed load leads to a more satisfactory description of the bed evolution. This finding opens important issues on how the inclusion of the nonlinear gravitational effects on the bed load can affect the morphodynamic evolution of complex bed topography occurring in natural rivers. To investigate this point, an application to the evolution of river bars is presented.

Citation: Francalanci, S., L. Solari, and M. Toffolon (2009), Local high-slope effects on sediment transport and fluvial bed form dynamics, *Water Resour. Res.*, *45*, W05426, doi:10.1029/2008WR007290.

1. Introduction

[2] The evaluation of the sediment transport on an arbitrarily sloping bed is a crucial aspects in any morphodynamic model: when the bed is inclined in both longitudinal and transversal directions, gravity plays an important role in sediment dynamics and hence on bed load transport [*Parker*, 1984; *Sekine and Parker*, 1992; *Kovacs and Parker*, 1994; *Nino and Garcia*, 1994a, 1994b; *Talmon et al.*, 1995; *Damgaard et al.*, 1997]. High bed slopes can be found near river banks, along bar fronts, in river bifurcations and in steep mountain streams.

[3] This problem has been recently investigated by *Seminara et al.* [2002] and *Parker et al.* [2003] through a nonlinear theoretical model which provided a vectorial description of the bed load transport on arbitrarily sloping beds at low Shields stress for local bed inclinations up to the angle of repose of the bed material. In the work by *Seminara et al.* [2002], it was theoretically shown that Bagnold's hypothesis, used by many models to estimate the average concentration of bed load particles, is not valid. Recognizing this failure, *Parker et al.* [2003] formulated an alternative model for the bed load on arbitrarily sloping beds using the experimental observations of *Fernandez Luque and van Beek* [1976]. The model is based on an entrainment formulation of the bed load, according to which at equilibrium the flux of sediments entrained by the flow is equal to the flux deposited. In this way, a dynamic rather than a static [*Bagnold*, 1956] equilibrium of the bed interface is postulated. Results suggest that linear formulations [*Ashida and Michiue*, 1972; *Engelund and Fredsoe*, 1976; *Wiberg and Smith*, 1985, 1989], devised for beds with small inclinations, when applied to an arbitrarily tilted bed, can lead to large underestimations of the intensity of the bed load transport. Moreover, when the bed is laterally tilted, bed load transport deviates from the direction of the applied bed shear stress due to gravity. The evaluation of this deviation is of great importance in various processes in which the lateral component of bed load transport plays a primary role, such as in the case of stream bank retreat, sediment sorting, bed topography in river bends, and river bifurcation. Linear formulations between the lateral component of bed load transport and lateral bed slope have been derived by various authors [*Engelund and Fredsoe*, 1976; *Ikeda*, 1982; *Struiksma et al.*, 1984; *Sekine and Parker*, 1992], but have been limited to the case of small lateral bed slopes.

[4] In the experimental work of *Francalanci and Solari* [2007] the average motion of particles saltating over a nonerodible, artificially roughened, planar bed was studied. The bed was arbitrarily inclined in both the longitudinal and transverse directions. The nonlinear theoretical model of *Parker et al.* [2003] was shown to provide an overall good agreement with the experimental observations. Since such a model is based on an iterative solution procedure, which can greatly increase the computational cost of the morphodynamic modeling, an interpolated equation for bed load transport intensity and direction was then derived by *Francalanci and Solari* [2008a].

[1] Center of Research and Advanced Education for Hydrogeological Risk Prevention, Retignano, Italy.
[2] Department of Civil and Environmental Engineering, University of Florence, Florence, Italy.
[3] Department of Civil and Environmental Engineering, University of Trento, Trento, Italy.

0043-1397/09/2008WR007290$09.00

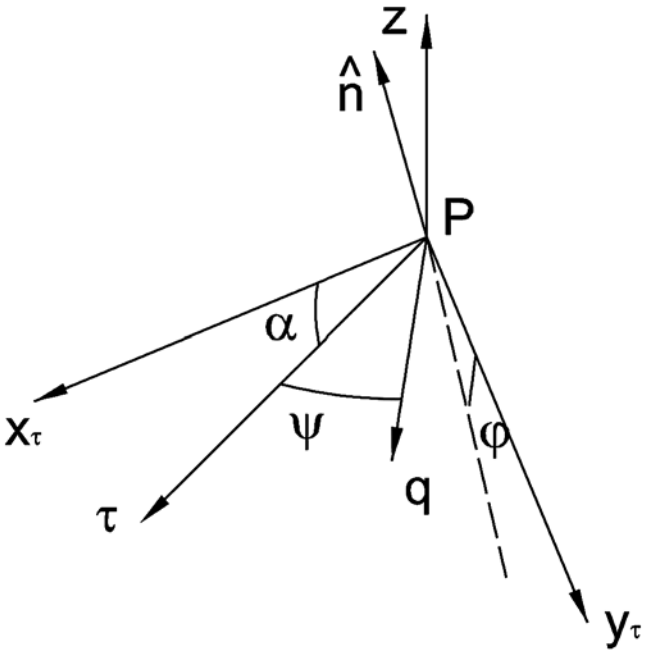

Figure 1. Notations.

[5] In the present work, we investigate the morphodynamic implication of the nonlinear formulation of bed load transport given by *Parker et al.* [2003]. To this end, we present an experimental study on the evolution of a mobile bed from its initial, laterally tilted configuration, to its final, laterally flat configuration, due to the gravity-driven lateral component of bed load transport. The initial configurations of the experiments presented in this paper are the same as those for experiments carried out over arbitrarily tilted nonerodible beds [*Francalanci and Solari*, 2007]. In the latter experiments the averaged values of shear stress profile, particle velocity, intensity, and the direction of bed load transport were determined. In the new set of experiments, the bed topography was measured at different times from the beginning of the run, giving a temporal description of the effect of sediment transport over an inclined bed. The experimental observations are then interpreted by considering the corresponding numerical solutions obtained through a three-dimensional model [*Vignoli*, 2005]. In order to assess the effect of different closure relationships for bed load transport, the numerical simulations have been repeated using the classical linear formulations (e.g., the formula of *Meyer-Peter and Müller* [1948]), the nonlinear formulation obtained by *Parker et al.* [2003], and the latter's linearized version.

[6] A further point to be clarified is how the inclusion of nonlinear gravitational effects (i.e., the effects of local high slopes) in the description of the bed load affects the morphodynamic evolution of the complex bed topography occurring in natural rivers [*Seminara*, 1998]. To discuss this point, we present an application to river bars, which typically display high slopes along the bar fronts. The above linear and nonlinear models are applied to study the formation and evolution of river bars in a straight channel. The differences among the results produced with the different models are then highlighted in terms of overall quantities (e.g., bar migration celerity and the maximum longitudinal and transversal inclinations).

[7] The rest of the paper is organized as follows: the next section states the problem of defining the appropriate sediment transport relationship over arbitrarily sloping beds; then, in section 3 the experimental setup is described and the numerical model is introduced. In section 4 the experimental observations are shown and compared with numerical results and the role of the transport relationship is highlighted. Finally, in section 5 the practical consequences are discussed, with special focus on bed form dynamics.

2. Formulation of the Problem

[8] In the present work the focus is on the evaluation of intensity and direction of the bed load as functions of the longitudinal and transversal slopes of the bed. Two dimensionless parameters have been shown to control the entrainment condition and the intensity of bed load, both interpreted in an average sense to rule out the intermittent character of the turbulent processes. The parameters are the Shields stress τ_* and the particle Reynolds number R_p, defined in the form:

$$\tau_* = \frac{|\boldsymbol{\tau}|}{(\rho_s - \rho)gD}, \qquad R_p = \frac{\sqrt{(s-1)gD^3}}{\nu}, \tag{1}$$

where ρ_s is the density of sediments, ρ is the density of water, $s = \rho_s/\rho$ is the relative density, D is the particle diameter (assuming that the sediment distribution can be described by a uniform size), ν is the kinematic viscosity, $\boldsymbol{\tau}$ is the average bed shear stress vector, and g is gravitational acceleration. In the following, we will consider the bed load transport vector per unit width, $\mathbf{q}$, made dimensionless using Einstein's scale

$$Q_0 = \sqrt{(s-1)gD^3}. \tag{2}$$

[9] Denoting unit vectors with a carat (ˆ), we consider a Cartesian coordinates system (x_τ, y_τ, z), centered at a given point P lying on the bed, with unit vectors ($\hat{\mathbf{x}}_\tau$, $\hat{\mathbf{y}}_\tau$, $\hat{\mathbf{k}}$), respectively (see Figure 1 for notations). z is the vertical axis, x_τ is the horizontal axis lying in the vertical plane ($\boldsymbol{\tau}$, $\hat{\mathbf{k}}$), while y_τ is the horizontal axis orthogonal to the plane ($\hat{\mathbf{x}}_\tau$, $\hat{\mathbf{k}}$). Note that the directions of the bed shear stress and of gravity provide the only two externally imposed directions to the problem; in particular note that the longitudinal axis x_τ may be at an arbitrary angle with the channel axis. The streamwise inclination α of the bed at any point P is defined as the inclination of the line resulting from the intersection of the bed surface with the plane ($\hat{\mathbf{x}}_\tau$, $\hat{\mathbf{k}}$); similarly the corresponding transverse inclination φ of the bed at P is defined as the inclination of the line resulting from the intersection of the bed surface with the plane ($\hat{\mathbf{y}}_\tau$, $\hat{\mathbf{k}}$). Note that these two lines are not in general orthogonal to each other. It is useful to introduce also a bed tangent reference system ($\hat{\mathbf{s}}$, $\hat{\mathbf{s}} \times \hat{\mathbf{n}}$) with the unit vector $\hat{\mathbf{s}}$ corresponding to the direction of bed shear stress $\boldsymbol{\tau}$ and the unit vector $\hat{\mathbf{n}}$ the upward normal to the bed.

[10] In the case of an arbitrarily (both longitudinally and transversally) tilted bed, gravity affects both the condition of the incipient motion and the bed load. The critical Shields

stress for the onset of sediment motion τ_{*c} on a tilted bed appears to be smaller than τ_{*c0} in the case of a flat bed; in the limiting case of a bed inclination equal to the angle of repose, τ_{*c} becomes zero. *Seminara et al.* [2002] showed that the ratio τ_{*c}/τ_{*c0} depends on the longitudinal and lateral bed inclinations; similar results have also been obtained by other authors [*Kovacs and Parker*, 1994; *Dey*, 2003].

[11] As regards the bed load vector, the presence of lateral inclination makes the bed load deviate from the direction of the bed shear stress; the angle between these two vectors is here called the deviation angle ψ. In this case, the bed load exhibits both a longitudinal component along $\hat{\mathbf{s}}$ and a transversal component along $(\hat{\mathbf{s}} \times \hat{\mathbf{n}})$.

[12] According to the nonlinear model of *Parker et al.* [2003], here approximated with the interpolating equations elaborated by *Francalanci and Solari* [2008a] (hereafter referred to as the NLM), the intensity of the bed load and the deviation angle take the following expressions:

$$|\mathbf{q}| = A_q(\alpha,\varphi)\cdot\left(\frac{\tau_*}{\tau_{*c0}}\right)^2 + B_q(\alpha,\varphi)\cdot\left(\frac{\tau_*}{\tau_{*c0}}\right) + C_q(\alpha,\varphi), \quad (3)$$

$$\psi = A_\psi(\alpha,\varphi)\cdot\left(\frac{\tau_*}{\tau_{*co}}\right)^{B_\psi(\alpha,\varphi)} \quad (4)$$

where the coefficients A_q, B_q, C_q, A_ψ and B_ψ are polynomial functions of the local bed inclinations α and φ. In particular, for α and φ from 0° up to 25°, A_q, B_q, C_q, A_ψ and B_ψ fall in the ranges (0, 0.017), (0, 0.041), (−0.022, 0.014), (0, 30.85), and (−0.48, −0.33), respectively. The negative values of B_ψ suggest that, as expected, the deviation angle decreases with τ_*.

[13] In linear formulations, strictly valid in the case of gentle slopes, it is assumed that gravity slightly affects the intensity and direction of the bed load with respect to the case of bed load q_0 due to a uniform flow over a flat bed; in other words,

$$\mathbf{q} = q_0[\hat{\mathbf{s}} + \tan\psi(\hat{\mathbf{n}} \times \hat{\mathbf{s}})] \quad (5)$$

with

$$\tan\psi = \frac{r}{\sqrt{\tau_*}}\tan\varphi, \quad (6)$$

where r is a constant.

[14] The linearized approximation of the *Parker et al.* [2003] nonlinear model (hereafter the L-NLM) leads to the following estimates:

$$r = \frac{\lambda_0\sqrt{\tau_{*c0}}}{\mu_{d0}} \quad (7)$$

and

$$q_0 = \frac{A}{\mu_{d0}}\left(\tau_* - \tau_{*c0}\right)\left(\sqrt{\tau_*} - \lambda_0\sqrt{\tau_{*c0}}\right). \quad (8)$$

In these expressions, λ_0 is a dimensionless coefficient that is a function of the ratio between the critical Shields stress for the cessation of the bed load motion and τ_{*c0}, A is a constant taking into account the logarithmic velocity profile near the wall, and μ_{d0} is the dynamic friction coefficient in the case of a flat bed. The numerical values of the coefficients used in the analysis are reported in section 4.

[15] Relationships of the same form as equation (8) have been obtained by *Ashida and Michiue* [1972], *Engelund and Fredsoe* [1976], and *Bridge and Bennett* [1992]. Linear relationships between the lateral component of bed load and the lateral bed slope, like equation (6), have been derived by various authors [*Ikeda*, 1982; *Engelund and Fredsoe*, 1976; *Struiksma et al.*, 1984; *Sekine and Parker*, 1992]; results of the various analyses differ in the forms taken by the coefficient in the linear relationship r, which appears to fall in the range $0.3 \div 0.6$ [*Talmon et al.*, 1995]. Note that, according to the linear models, the angle of deviation is not affected by the longitudinal bed slope. This is in contrast to the NLM (equation (4)) which shows instead that, for given applied Shields stress and lateral bed inclination, ψ decreases with the longitudinal bed inclination [*Francalanci and Solari*, 2008a]. Moreover, according to the NLM ψ decreases with τ_* at a lower rate than that predicted by the LM (equation (6)).

[16] It can be seen that the NLM predicts a much faster growth of the bed load intensity with τ_* than L-NLM (8). Similarly, the rate of increase of $\mathbf{q}$ with the longitudinal and transversal inclinations is much larger in the NLM compared to L-NLM. The rest of the paper is devoted to assessing the performance of the NLM, L-NLM, and usual linear model by testing their ability to reproduce the experimental observations of bed evolution of an initially arbitrarily tilted bed.

3. Materials and Methods

3.1. Experimental Setup

[17] The evolution of the mobile bed was investigated in a free surface laboratory flume. The experiments were carried out in a tilting, recirculating flume, 10 m long, 0.365 m wide, and 0.45 m deep, equipped for clear water flow rates up to 28 l/s and slope adjustment up to 5°. For practical reasons, in the reach under investigation the flume was narrowed and the employed width was 0.225 m. Water flow was supplied at one end of the flume from a centrifugal pump and the water discharge was monitored by an electromagnetic flowmeter.

[18] The sediment particles were fed at a constant rate by means of a sediment feeder. These particles satisfied the following requirements for the bed slopes investigated in this study: mobility at low Shields stress; ratio of water depth to particle size sufficiently high to allow particle saltation, even in the case of high bed slope; and relatively high friction angle. The selected material was represented by steel particles with a density of 7850 kg/m^3, shaped like disks with almost uniform size of 3 mm maximum diameter and 0.6 mm thickness. The use of steel particles with a higher density, compared to the common fluvial sediments, allowed one to perform sediment transport experiments on a free surface laboratory flume with high local inclinations of the bed and sufficiently high water depth. The nonspherical shape allowed simpler particles disposition according to a given transversal inclination. In spite of the differences, the

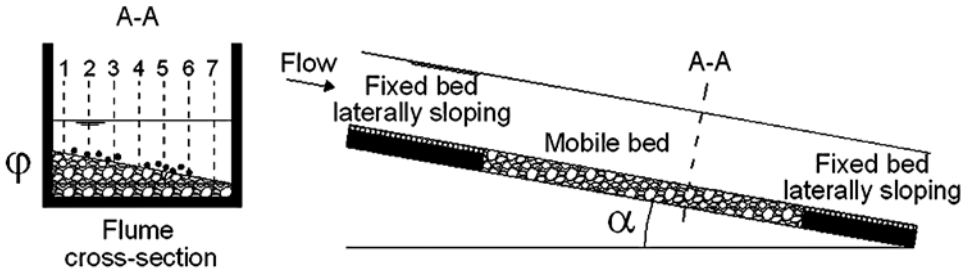

Figure 2. Sketch of the setup for the mobile bed experiments.

steel particles have been observed to show very reasonable saltation dynamics compared to the natural sediments [*Francalanci and Solari*, 2007, 2008b]: the average saltation height is on the order of 1.5–3 times the particle diameter, as reported by various authors [*Abbott and Francis*, 1977; *Lee and Hsu*, 1994; *Nino and Garcia*, 1994a; *Hu and Hui*, 1996; *Sekine and Kikkaua*, 1992; *Lee et al.*, 2000], and the average particle velocity appears to be in agreement with experimental values obtained by *Francis* [1973] and *Nino and Garcia* [1994a], who have also employed natural sediments. Moreover, the general good agreement of *Parker et al.* [2003] model, devised for spherical sediments, with the results of *Francalanci and Solari* [2007] suggests that the shape of the particles has no more than a second-order effect on the bed load transport.

[19] A sketch of the experimental setup is shown in Figure 2. For each experiment, the mobile bed was initially shaped according to a given longitudinal α and transversal φ inclination. The mobile bed reach was 5 m long, and was located between two 0.2 m fixed bed zones having the same longitudinal and transversal inclination of the mobile bed at the initial condition; in this way the mobile bed was initially leveled with both the upstream and downstream fixed beds. In order to maintain the same bed roughness of the mobile bed, the steel particles were glued on the surfaces of the two fixed bed zones. The employed setup was designed to achieve an initial uniform flow over the fixed and mobile bed.

[20] At the beginning and at the end of the experiments, the bed elevation was measured along different cross sections. These cross sections were located at intervals of 50 cm in the upstream part of the mobile bed and 25 cm in the downstream part, where the equilibrium configuration was reached, as shown in Figure 3. For each cross section, the bed elevation was measured using a point gauge in 7 verticals, spaced about 3 cm apart (see Figure 2).

3.2. Experimental Procedure

[21] The experiments were conducted using different longitudinal and transversal inclinations of the bed. At the beginning of each experiment, the transversal slope of the fixed bed was set and the mobile bed was shaped accordingly. Then, the initial configuration of the bed elevation was measured. After the preparation, the experiments were performed according to the following procedure. First the flow discharge was adjusted to the assigned value: during this transient period the mobile bed was not allowed to evolve by means of a fine grid. When the latter was removed, the experiment started and the evolution of the bottom topography was observed using a video recorder. For each initial configuration, several experiments with different durations were performed and the bed elevation was measured at the end of each run, in dried condition. The transient period at the end of the run did not influence the dried bed configuration.

[22] The bottom topography at the end of each run was taken to be representative of the configuration at that given time in longer experiments; in this way, we were able to reconstruct the temporal evolution of the bed topography by considering separate runs. Additional data regarding the flow velocity profiles, the applied bed shear stresses, and the particle velocity were inferred from previous experimental activity on nonerodible beds [*Francalanci and Solari*, 2007].

3.3. Numerical Model

[23] In order to evaluate whether the proposed sediment transport models can satisfactorily reproduce the experimental observations, we employed linear and nonlinear closure relationships in a three-dimensional numerical model. The adopted model, developed by *Vignoli* [2005], is based on the semi-implicit procedure proposed by *Casulli and Cattani* [1994], according to which the nonlinear advective terms in the momentum equations are discretized using a Lagrangian approach, while the pressure term and the viscous terms are solved implicitly within an Eulerian framework. The approach has been modified in this work to account for the no-slip condition at the bed. The spatial mesh is given by a staggered grid and consists of rectangular boxes within a boundary-fitted approach.

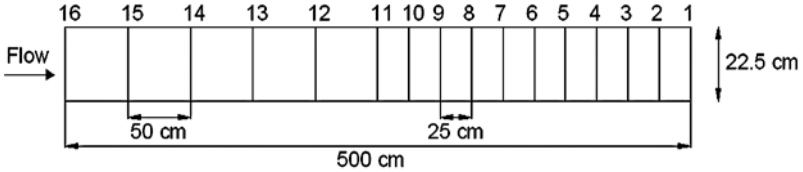

Figure 3. Longitudinal plan view of the mobile bed reach. The numbers specify measuring cross-section locations.

Table 1. Initial Experimental Conditions[a]

Run Code	α (deg)	φ (deg)	Q_w (l/s)	Time (s)
Run 1	1.72	10	15.4	180–270–360–540
Run 2a	5	5	5.98	30–60–210
Run 2b	5	5	7.5	30–180
Run 3	5	10	7.02	30–60–150–210
Run 4	10	5	4.5	20–40–72

[a]Longitudinal bed inclination α, transversal bed inclination φ, water discharge Q_w, and duration of the run. The characteristic Froude numbers are indicated in Table 2.

Moreover, a suitable logarithmic vertical coordinate is introduced such that the grid density decreases from the bed to the free surface. This logarithmic vertical coordinate follows the gradient of the velocity profile and hence minimizes the numerical truncation errors, achieving better accuracy with the same number of grid points. The bed evolution is governed by the sediment continuity equation (Exner equation) and is solved with a decoupled procedure using the hydraulic variables obtained from the continuity and momentum equations for the liquid phase. The resulting numerical scheme has been shown to adequately represent the hydrodynamics of fluvial systems and the role of sediment transport in the development of bed topography [*Vignoli and Tubino*, 2002; *Francalanci et al.*, 2006; *Toffolon and Vignoli*, 2007].

[24] The model considers a straight channel with vertical banks, characterized by a cohesionless bed and constant width B; x is the longitudinal axis, directed downstream according to the average bed slope S, y is the transversal axis, and z the vertical one, directed upward. The equations are solved in dimensionless form, adopting suitable scaling factors; that is, the planimetric coordinates are scaled to the channel width B; the vertical coordinate, the local free surface elevation h, the bed elevation η, and the flow depth H are scaled to a reference flow depth H_0; and the velocity components are scaled to the reference flow velocity. Furthermore a characteristic convective time scale $T_0 = B/U_0$

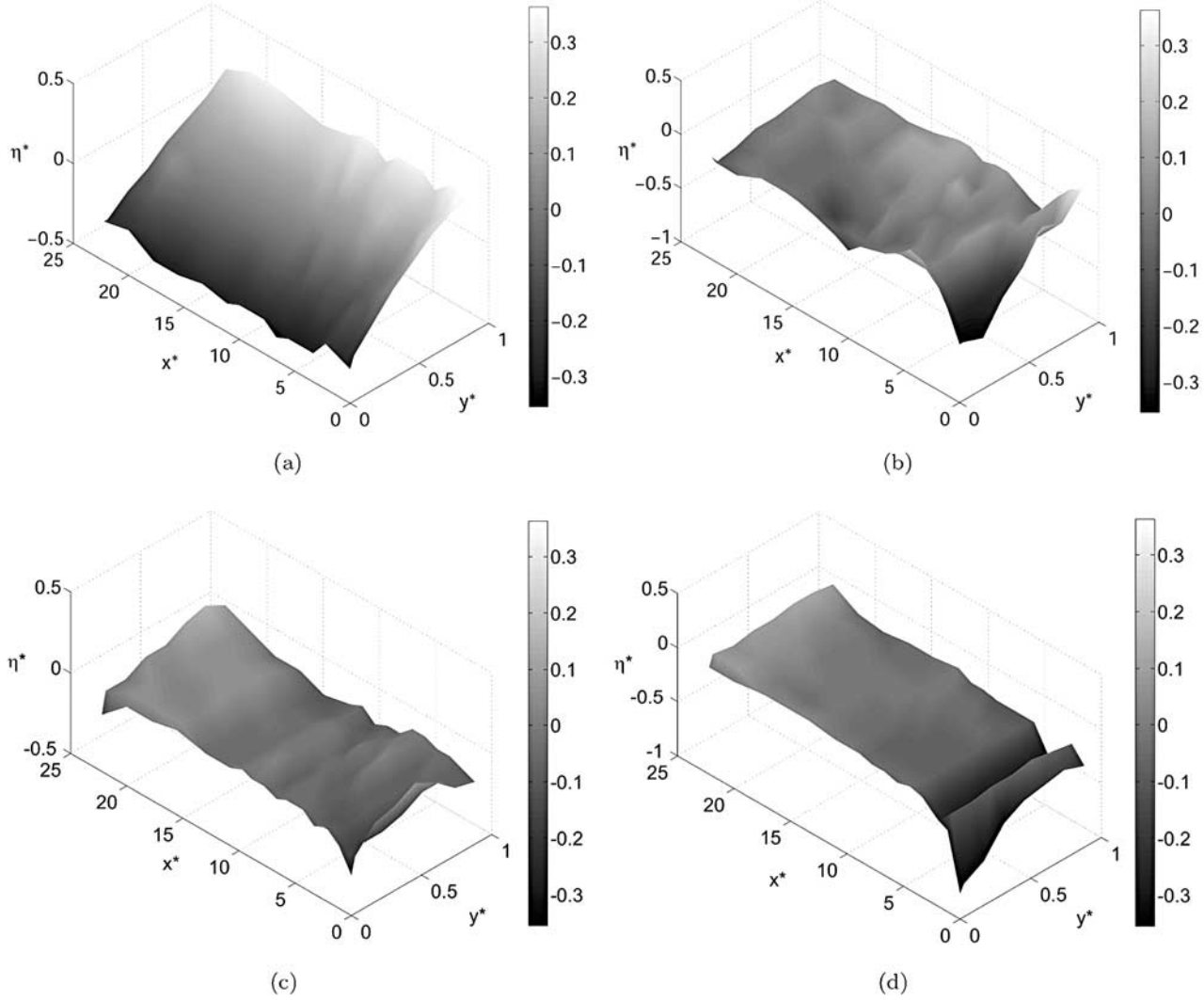

Figure 4. Configuration of the bed elevation for experimental run 2a in dimensionless variables. (a) Initial configuration, (b) configuration after 30 s, (c) configuration after 60 s, and (d) configuration after 210 s.

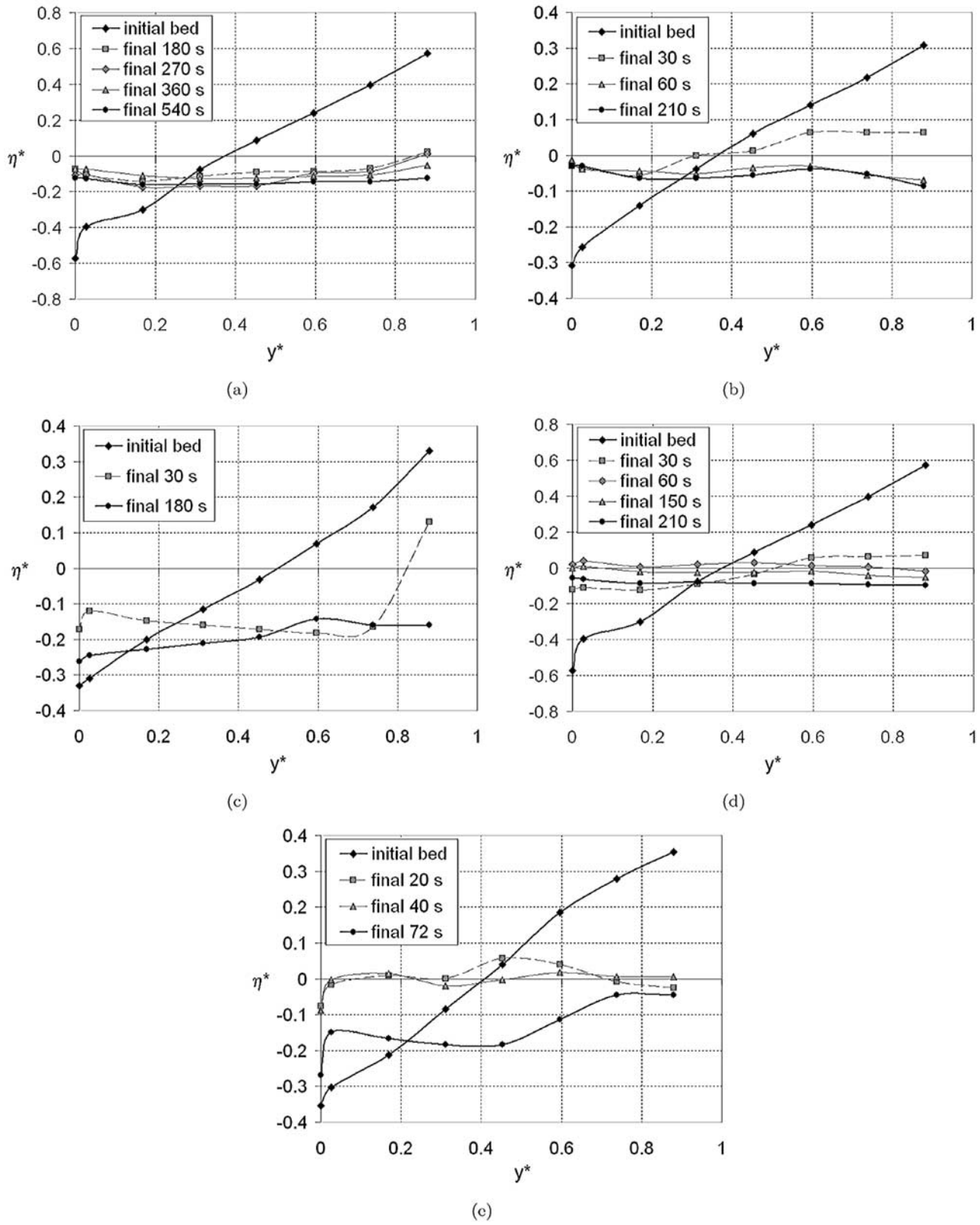

Figure 5. Evolution of the bed elevation along the equilibrium cross section, averaged in the cross sections from 1 to 10 located in the downstream end of the mobile bed, for the experimental runs. (a) Run 1, (b) run 2a, (c) run 2b, (d) run 3, and (e) run 4.

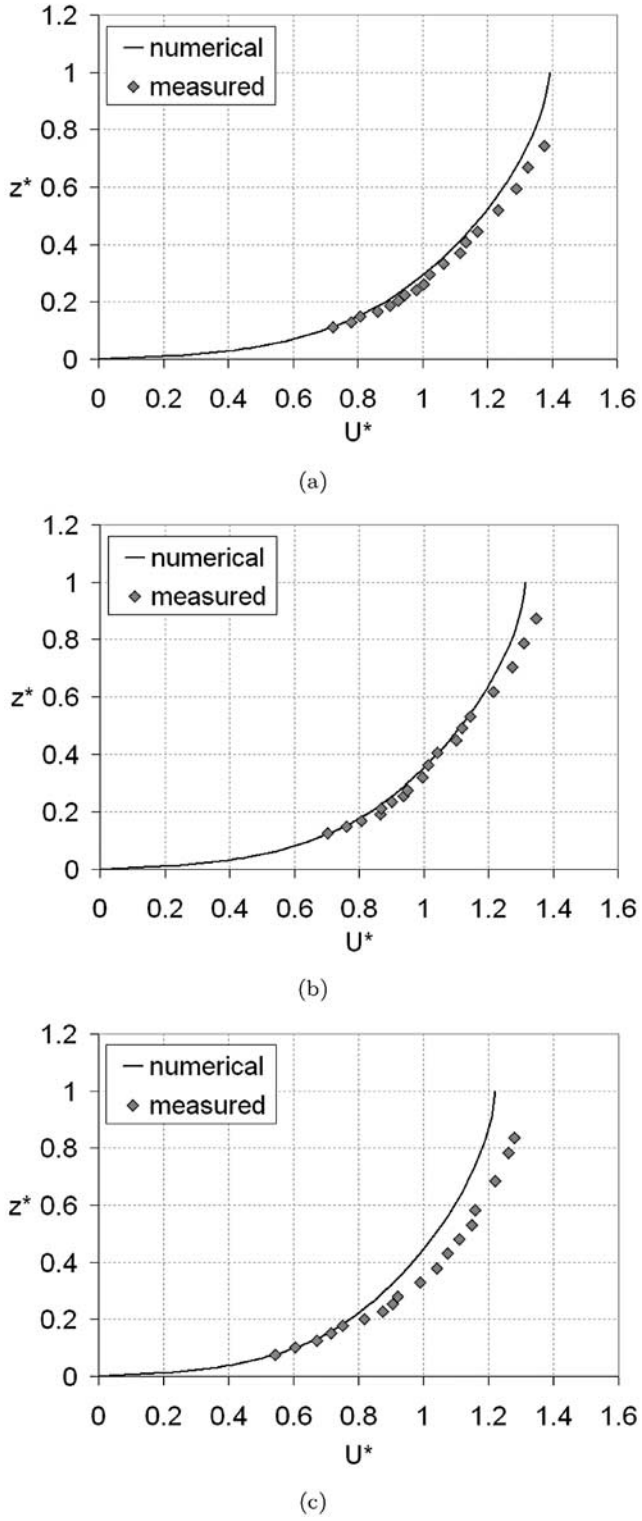

Figure 6. Comparison between the measured flow velocity profiles and the simulated ones, taken at a distance $y^* = y/B$ from the wall (run 2a). (a) $y^* = 0.22$, (b) $y^* = 0.4$, and (c) $y^* = 0.58$.

is introduced. The reference values U_0 and H_0 refer to cross-sectional averaged velocity and depth of the uniform flow, for a given discharge, bed slope and sediment size. The simulation conditions are completely determined once R_p and the following dimensionless parameters (aspect ratio, dimensionless grain size, and Shields parameter) are given:

$$\beta = \frac{B/2}{H_0}, \qquad D_s = \frac{D}{H_0}, \qquad \tau_* = \frac{C_{f0}U_0^2}{(s-1)gD}, \tag{9}$$

where C_{f0} is the friction coefficient of the reference uniform flow. The half width $B/2$ is used in the definition of β in analogy with previous works on bed form development [e.g., *Colombini et al.*, 1987]. Hereafter a star ($*$) will denote dimensionless variables.

[25] In dimensionless form, assuming shallow water, hydrostatic pressure distribution and keeping only significant turbulent flux, the Reynolds equations along the longitudinal and transversal direction, the flow continuity equation and the sediment continuity equation read:

$$\frac{\partial U^*}{\partial t^*} + U^*\frac{\partial U^*}{\partial x^*} + V^*\frac{\partial U^*}{\partial y^*} + (2\beta)W^*\frac{\partial U^*}{\partial z^*} - (2\beta)\sqrt{C_{f0}}\frac{\partial}{\partial z^*}\left(\nu_T^*\frac{\partial U^*}{\partial z^*}\right) + \frac{1}{F_0^2}\frac{\partial H^*}{\partial x^*} - (2\beta)\frac{S}{F_0^2} = 0, \tag{10}$$

$$\frac{\partial V^*}{\partial t^*} + U^*\frac{\partial V^*}{\partial x^*} + V^*\frac{\partial V^*}{\partial y^*} + (2\beta)W^*\frac{\partial V^*}{\partial z^*} - (2\beta)\sqrt{C_{f0}}\frac{\partial}{\partial z^*}\left(\nu_T^*\frac{\partial V^*}{\partial z^*}\right) + \frac{1}{F_0^2}\frac{\partial H^*}{\partial y^*} = 0, \tag{11}$$

$$\frac{\partial U^*}{\partial x^*} + \frac{\partial V^*}{\partial y^*} + (2\beta)\frac{\partial W^*}{\partial z^*} = 0, \tag{12}$$

$$(1-\lambda_p)\frac{\partial \eta^*}{\partial t^*} + \Theta\left(\frac{\partial q_x^*}{\partial x^*} + \frac{\partial q_y^*}{\partial y^*}\right) = 0, \tag{13}$$

where (U^*, V^*, W^*) denote the dimensionless velocity components, S is the longitudinal channel slope, $F_0 = U_0/\sqrt{gH_0}$ is the Froude number of the reference flow, λ_p is the bed porosity, and $\Theta = Q_0/(U_0H_0)$, where Q_0 is the Einstein's scale for sediment transport given by equation (2). Hence $q_x^* = q_x/Q_0$ and $q_y^* = q_y/Q_0$ are the longitudinal and lateral components of the dimensionless bed load vector. More-

Table 2. Characteristic Parameters Used in the Numerical Simulation of the Experimental Runs[a]

Run Code	H_0 (m)	U_0 (m/s)	C_{f0} (−)	F_0 (−)
Run 1	0.050	1.37	11.3	1.95
Run 2a	0.021	1.30	9.7	2.87
Run 2b	0.024	1.41	9.9	2.93
Run 3	0.024	1.42	9.9	2.93
Run 4	0.014	1.41	9.1	3.81

[a]Reference flow depth H_0, reference flow velocity U_0, and resistance coefficient C_{f0}. The Froude number F_0 is indicated as a reference for the experimental conditions.

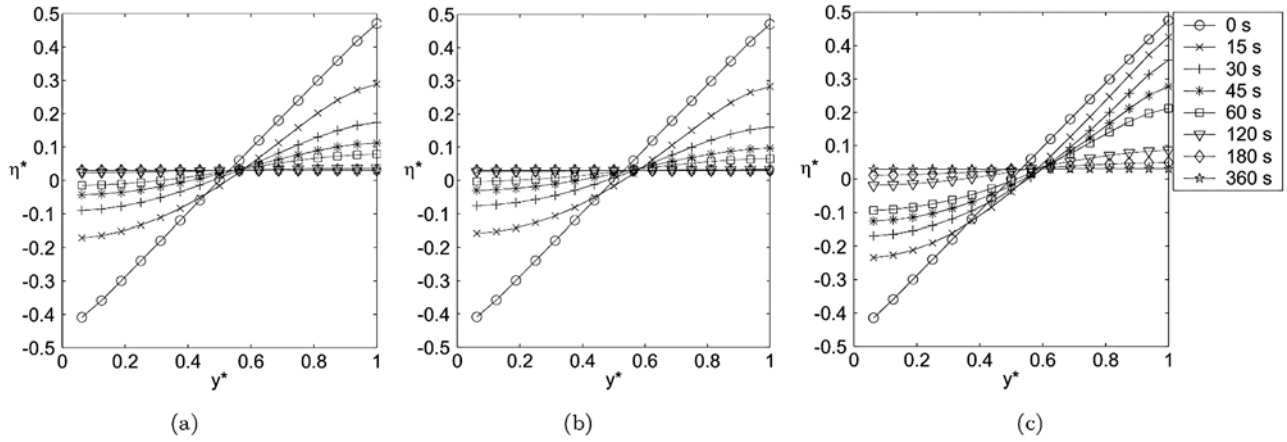

Figure 7. Numerically simulated evolution of the dimensionless bed elevation η^* in the cross section (run 2a): comparison between (a) NLM, (b) L-NLM, and (c) L-MPM.

over, $\nu_T^* = \nu_T/(\sqrt{C_{f0}}U_0H_0)$ is the dimensionless structure of eddy viscosity, where we have introduced the usual Fickian closure for turbulent fluxes. The eddy viscosity ν_T is evaluated according to *Dean* [1974] on the basis of the local hydrodynamic values, with the assumption that the slowly varying character of the flow field, both in space and in time, leads to a sequence of quasi-equilibrium states. The usual boundary conditions are assigned to the flow field: the dynamic condition at the free surface (imposing vanishing stresses), no slip at the bottom, and the kinematic conditions at both vertical boundaries (imposing continuity of the normal component of velocity and surface displacement).

4. Results

[26] The experimental observations of the evolution of the mobile bed are described and compared with the three-dimensional numerical simulations obtained employing (1) the nonlinear model by *Parker et al.* [2003] (NLM), here approximated with the interpolating relationships (3) and (4) proposed by *Francalanci and Solari* [2008a]; (2) its linearized version (L-NLM) in the form given by (5) and (6); and (3) an example of the linear models, which is here implemented in the case (hereafter L-MPM) of the widely employed classical bed load transport equation of *Meyer-Peter and Müller* [1948], hereafter referred to as L-MPM. The L-MPM is used in the form revised by *Wong and Parker* [2006], coupled with the relationship (6) proposed by *Ikeda* [1982] to estimate the transversal component of the bed load transport.

[27] The bed load model is applied with the following values of the main parameters, estimated by means of the experimental results from a study of bed load over a nonerodible sloping bed [*Francalanci and Solari*, 2007]: dynamic friction coefficient in the case of a horizontal bed $\mu_{d0} = 0.3$, angle of repose of sediments $\phi = 35°$, critical Shields stress for the onset of sediment motion on a flat bed $\tau_{c0}^* = 0.03$, and $\lambda_0 = 0.7$. The same values adopted by *Parker et al.* [2003] are used for the remaining parameters, based on the best fit with the experimental results of *Fernandez Luque and van Beek* [1976]. The values here adopted lead to $A = 7.7$ in equation (5) and $r = 0.4$ in equation (6). For the purpose of comparison the latter value is also maintained in the relationship of *Ikeda* [1982].

4.1. Experimental Observations

[28] The initial conditions for the experimental runs are reported in Table 1. In particular, the longitudinal inclination of the bed varied from 1.72° to 10° and two transversal

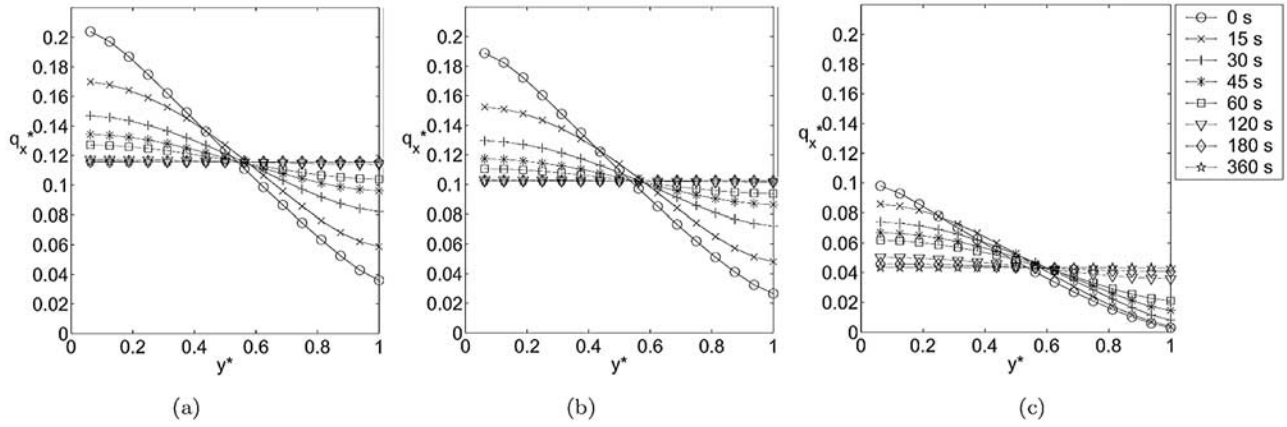

Figure 8. Numerically simulated evolution of the dimensionless longitudinal bed load transport q_x^* in the cross section (run 2a): comparison between (a) NLM, (b) L-NLM, and (c) L-MPM.

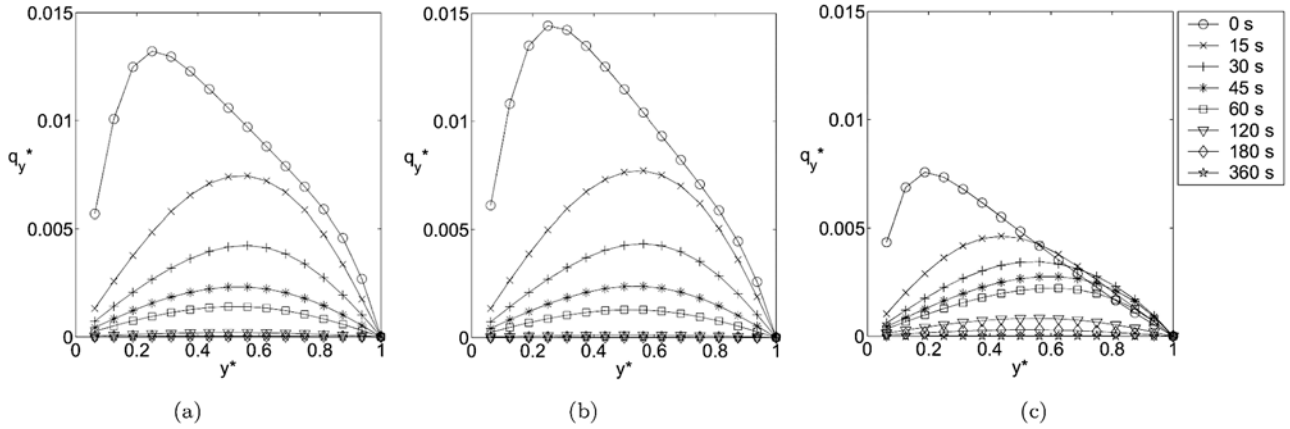

Figure 9. Numerically simulated evolution of the dimensionless transversal bed load transport q_y^* in the cross section (run 2a): comparison between (a) NLM, (b) L-NLM, and (c) L-MPM.

inclinations were chosen (5° and 10°). In order to relate the initial conditions of the mobile bed with the complete set of measurements collected during the nonerodible bed experiments, the initial configurations of the present experiments were the same as those of *Francalanci and Solari* [2007]. In this way, the bed shear stress distribution, average flow velocity profiles, particle velocity, and bed load transport rate were already known at the beginning of each experiment. The experimental runs 2b and 4 were performed with a shorter mobile bed reach, namely 1.5 m instead of 5 m; this was due, in the case of run 4, to the high longitudinal bed inclination of 10° which did not allow for a longer length. Moreover, an upper limit to the possible bed inclinations was set by the need for the flow to wet the entire cross section, in this way the bed flattening was only produced by the lateral component of bed load transport and not by other mechanisms related to mass failure of the bed.

[29] As a first example, the morphodynamic evolution of the cross sections is shown in Figure 4 for run 2a at different times until the equilibrium configuration was attained. After 30 s an erosion phenomenon was observed at the beginning of the mobile bed due to the transition from fixed (laterally inclined) bed to erodible bed. After 60 s, the mobile bed was already close to the equilibrium configuration, which was observed after 210 s. The local scour phenomenon in the upstream part of the mobile bed increased because of the difficulties in maintaining the sediment feeding in equilibrium with the bed load transport capacity, while in the downstream bed the laterally flat equilibrium cross section was observed. This local scour was confined to a narrow region and did not affect the flattening evolution of the bed in the downstream part of the mobile reach.

[30] We now focus on the downstream portion of the mobile reach, where the scour formed in the transition from fixed to mobile bed was not present. In particular, the measured bed elevations in cross sections 1 to 10 (as defined in Figure 3), located in the downstream end of the mobile bed, were averaged and the most significant features of the evolution are here summarized.

[31] Run 1 was performed with a relatively low longitudinal inclination. The topography of the bed was obtained for 4 different durations of the experiment. The first part of the mobile bed was affected by a local erosion phenomenon, but equilibrium was achieved at the end of the mobile bed reach. The mobile bed reached the transversal equilibrium configuration after about 540 s, as shown in Figure 5a.

[32] Run 2 was carried out with two different flow discharges. The experimental results of run 2a and run 2b are shown in Figures 5b and 5c, respectively. Run 2b exhibited a faster bed evolution because of the stronger

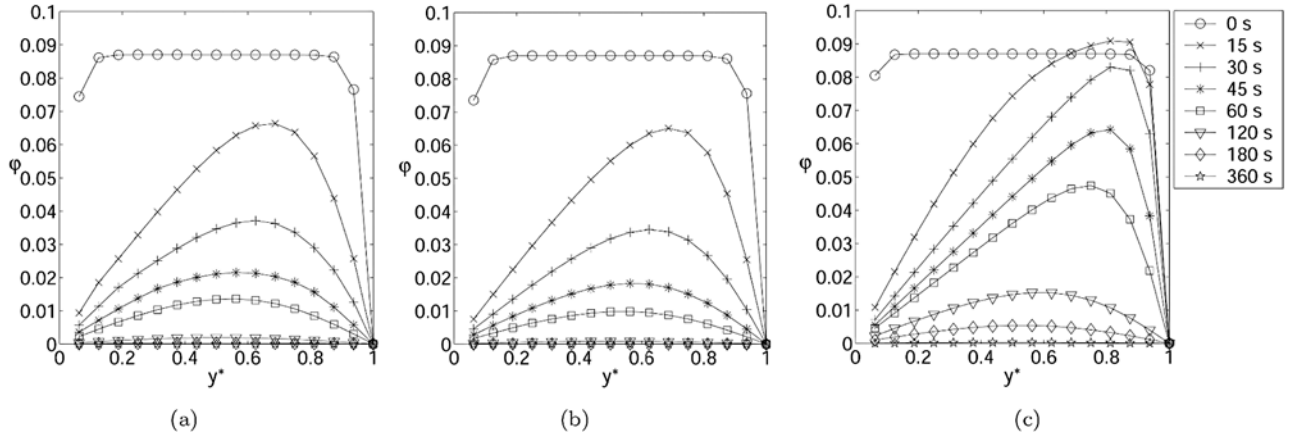

Figure 10. Numerically simulated evolution of the transversal bed inclination φ in the cross section (run 2a): comparison between (a) NLM, (b) L-NLM, and (c) L-MPM.

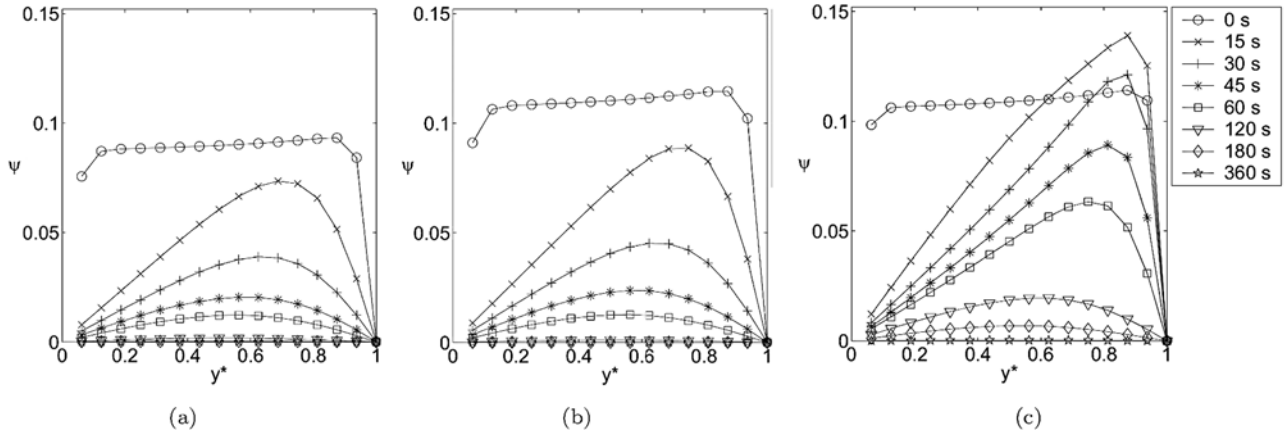

Figure 11. Numerically simulated evolution of the deviation angle ψ in the cross section (run 2a): comparison between (a) NLM, (b) L-NLM, and (c) L-MPM.

intensity of the bed load transport associated with the larger flow discharge.

[33] Run 3 was performed with a higher transversal inclination than run 2. Under these conditions the mobile bed reached the equilibrium configuration, after which a slow, uniformly distributed erosion phenomenon was observed in the equilibrium cross section (Figure 5d). This change was due to a variation of the longitudinal bed slope associated to the adjusted bed load discharge input.

[34] Run 4 was performed with a high longitudinal inclination ($\alpha = 10^\circ$), with a mobile bed reach of 1.5 m long. In this experiment the time evolution of the phenomenon was very rapid and hence the bottom topography was difficult to control and measure. The final profiles along the cross section are shown in Figure 5e.

4.2. Numerical Results and Comparison

[35] We now consider the results of the three-dimensional numerical model for the bed evolution, employing the different closure relationships (NLM, L-NLM and L-MPM) to evaluate the bed load transport. The numerical model requires some parameters, which can be calculated if the system geometry (width B, cross-sectional averaged water depth H_0, initial bed elevation η) and the particle characteristics are known. Several closure relationships have been proposed in the literature to estimate the resistance coefficient C_{f0} as a function of D_s and τ_*, but this parameter remains somewhat uncertain. Here, C_{f0} is calibrated by fitting the flow velocity profiles on a nonerodible bed measured by *Francalanci and Solari* [2007]. The measured flow velocity profiles along three verticals at a distance 0.22B, 0.4B and 0.58B from the left side wall, under the experimental conditions of run 2a (initial longitudinal inclination $\alpha = 5^\circ$, transversal inclination $\varphi = 5^\circ$), are compared with the model estimates in Figure 6. The agreement appears quite satisfactory especially in the proximity of the bed. Numerical simulations were carried out for each of the experimental run conditions (Table 2). Although Figure 6 includes only the results of run 2a, similar results were obtained for the other experimental runs. The numerical results are expressed in terms of the dimensionless quantities introduced in section 3.3.

[36] The modeled behavior of bed elevation in the cross section is shown in Figures 7a–7c. Figures 7a–7c show that the evolution according to *Meyer-Peter and Müller* [1948] in the revised form proposed by *Wong and Parker* [2006] (L-MPM) is slower than that predicted by both the NLM and L-NLM. In particular, all the formulations correctly predict that the final equilibrium configuration is laterally flat and is reached asymptotically in time, but the NLM

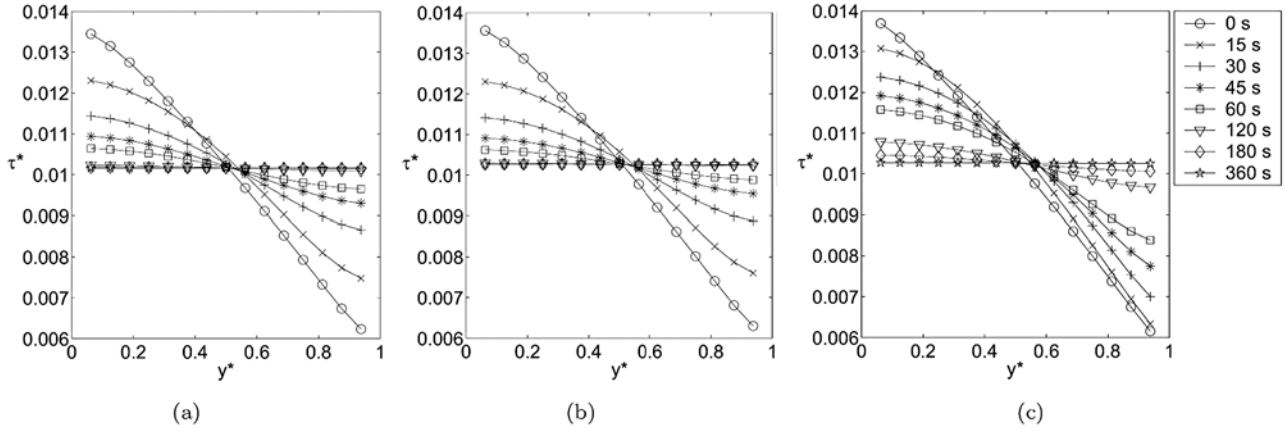

Figure 12. Numerically simulated evolution of the dimensionless bed shear stress $\tau^* = |\boldsymbol{\tau}|/(\rho U_\delta^{*2})$ in the cross section (run 2a): comparison between (a) NLM, (b) L-NLM, and (c) L-MPM.

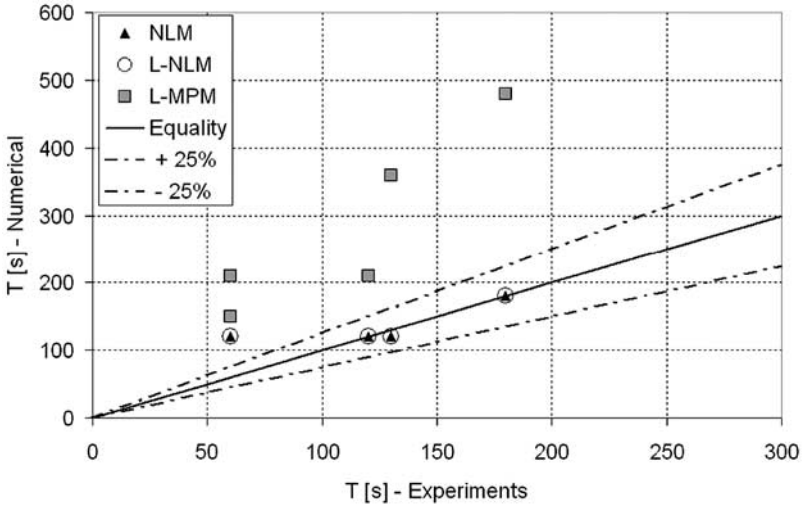

Figure 13. Comparison of the flattening time obtained from the experiments (horizontal axis) with the numerical results (vertical axis: NLM, L-NLM, and L-MPM formulations).

reveals that such a condition is attained in about one minute, while the L-MPM predicts that the flattening process occurs in several minutes. The observed bed evolution displayed in Figure 5b shows that the bed had already reached a flat configuration after 60 s. This finding suggests that both the NLM and L-NLM provide a better interpretation of the experimental observations than does the L-MPM.

[37] This observation is due to the different behavior of the bed load relationships. For the conditions of run 2a, the intensity of the bed load in the longitudinal direction according to the NLM is about twice that predicted by the L-MPM (see Figure 8). Note that the L-NLM predicts a bed load transport that is very similar, although slightly smaller, than that obtained with the NLM; this is due to the fact that the two models present significant differences only in the case of high bed inclinations, both longitudinal and transversal [*Francalanci and Solari*, 2008a].

[38] The transversal bed load transport (Figure 9) is the highest in the initial configuration of the bed, then decreases to zero when the bed is laterally flat. All the formulations predict that q_y^* attains a maximum in the central part of the cross section at the beginning of the experiment, and then decreases during the experiment. The predicted decrease of q_y^* is much faster for the NLM and L-NLM than for the L-MPM.

[39] The transversal bed inclination φ (Figure 10) is highest in the initial configuration and then decreases. Higher slopes are predicted toward the shallower part of the cross section where q_y^* appears smaller. Note that, unlike the NLM and L-NLM models, the L-MPM predicts that φ slightly increases during the initial part of the experiment, at least in a small portion of the entire cross section, which is due to the very small values of q_y^* which prevent part of the cross section from evolving.

[40] The deviation angle ψ (Figure 11) predicted by all the formulations appears very similar at the beginning of the run. During the flattening process ψ decreases from the initial value to become zero and shows a maximum value within the cross section due to the wall effects, which do not allow lateral sediment transport. In the case of the NLM and L-NLM the deviation angle progressively decreases in time at similar rates, while the L-MPM predicts a ψ that first increases in the shallower part of the cross section and then trends to zero.

[41] The bed shear stress is similarly decreasing (Figure 12), consistent with the time evolution of the previous quantities, and at the end of the run it reaches a value similar to the other formulations.

[42] Finally, the flattening time is estimated, defined as the time required for the bed to reach the laterally flat configuration. As the process is numerically asymptotic in time, the bed is assumed to be nearly horizontal in the transversal direction when the transversal inclination is less then 10^{-7}. A comparison between the experimental and numerical flattening time is shown in Figure 13. It appears that the flattening time is generally well predicted by both the NLM and L-NLM, while it is generally overestimated by the L-MPM. In the cases of run 3 and run 4 which exhibited the shortest flattening times, the numerical predictions by both the NLM and L-NLM appear larger than the experimental observations. This may be due to the difficulties of estimating the flattening time because of the lack of experimental observations at the early stages of the experiment.

5. Discussion

[43] To further elucidate the gravitational effects on bed load transport and river morphodynamics, we study the

Table 3. Dimensionless Parameters for the Numerical Simulations of Alternate Bars

Numerical Run	β	λ	R_p	D_s	τ_*
1	18	0.2	11000	0.01	0.1
2	18	0.2	11000	0.01	0.15
3	18	0.2	11000	0.01	0.2
4	18	0.2	11000	0.02	0.1
5	18	0.2	11000	0.02	0.15
6	18	0.2	11000	0.02	0.2
7	18	0.2	11000	0.04	0.1
8	18	0.2	11000	0.04	0.15
9	18	0.2	11000	0.04	0.2

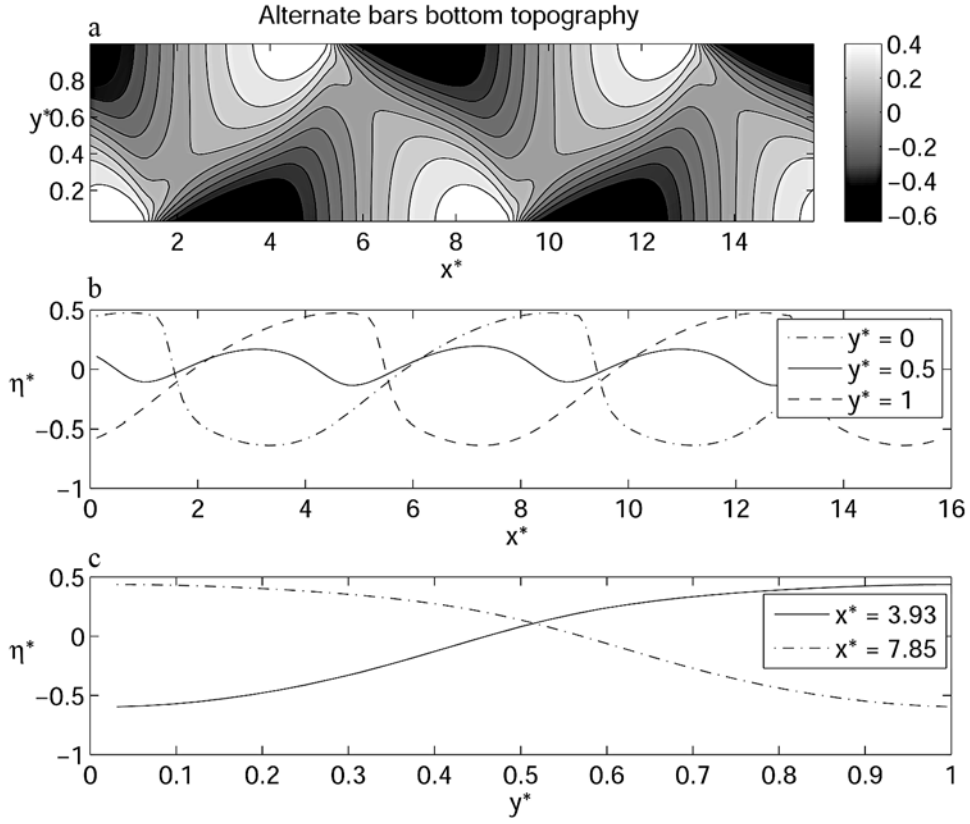

Figure 14. Example of alternate bars at equilibrium condition in the case of the NLM formulation (numerical run 8: R_p = 11000, β = 18, λ = 0.2, D_s = 0.04, and τ_* = 0.15): (a) dimensionless bed topography $\eta^*(x^*, y^*)$; (b) longitudinal bed profile $\eta^*(x^*)$ at y^* = 0, y^* = 0.5 and y^* = 1; and (c) lateral bed profile $\eta^*(y^*)$ at x^* = 3.93 and x^* = 7.85.

impact of the sediment transport closure on the dynamics of alternate bars, which are quite common in gravel bed rivers. River bars can locally display relatively high bed inclinations, especially along the riffle and the diagonal front; therefore it can be expected that a nonlinear description of gravitational effects on bed load transport can play some role in the definition of this morphology. To investigate the latter point, we employed the numerical model described in section 3.3 to simulate the dynamics of alternate bars in a straight channel. Different bed load formulations were used

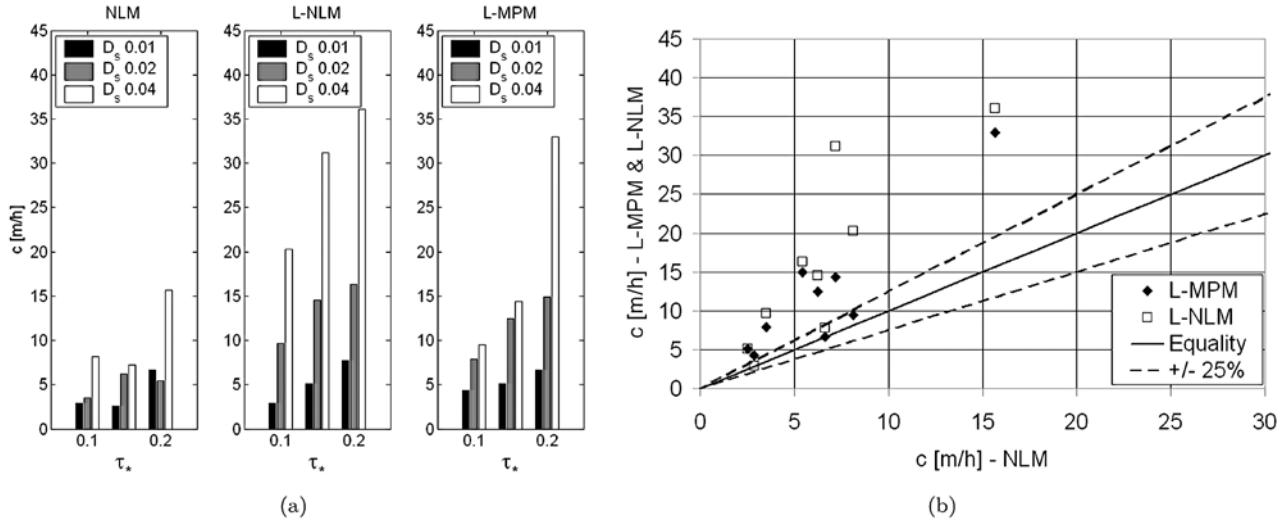

Figure 15. Alternate bars characteristics obtained from numerical simulations using different bed load closures: (a) dimensional bar celerity and (b) comparison of the celerity obtained with the linear (vertical axis: L-MPM and L-NLM) and nonlinear (horizontal axis: NLM) formulations.

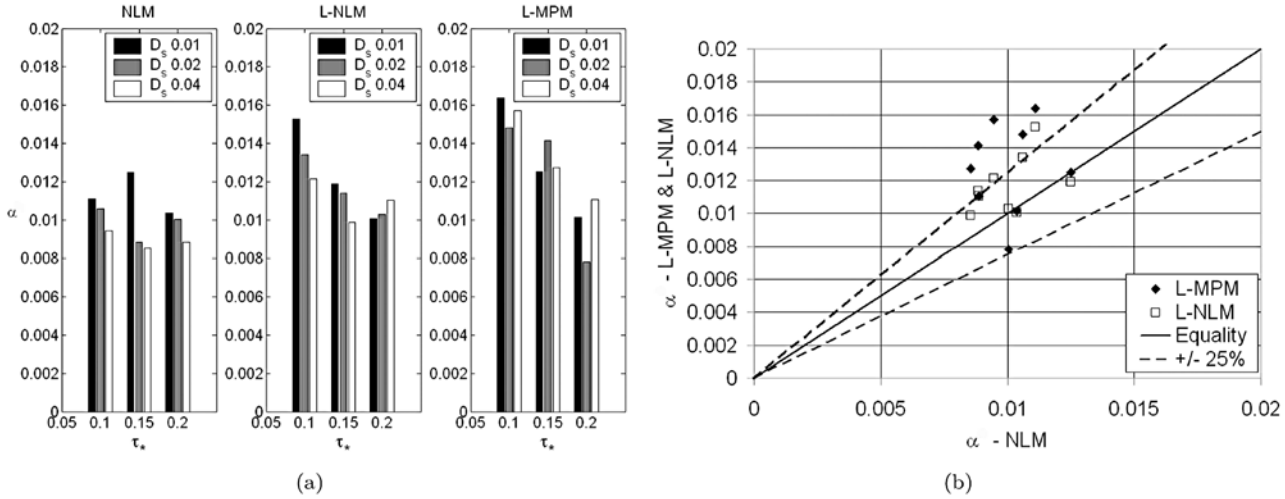

Figure 16. Alternate bars characteristics obtained from numerical simulations using different bed load closures: (a) longitudinal inclination and (b) comparison of the maximum longitudinal bed inclination obtained with the linear (vertical axis: L-MPM and L-NLM) and nonlinear (horizontal axis: NLM) formulations.

to account for the gravitational effects in both a nonlinear and a linear manner. Numerical simulations were carried out using the dimensionless parameters defined in (1) and (9) for input data typical of gravel bed rivers [see, e.g., *Parker et al.*, 2007], namely $\tau_* = 0.1, 0.15, 0.2$, bed sediment size $D = 2$ cm in the range of gravel with the particle Reynolds number $R_p = 11000$, and dimensionless grain size $D_s = 0.01$, 0.02, 0.04. The aspect ratio was fixed at a relatively high value ($\beta = 18$) in order to assure bar growth in each numerical experiment. The channel length L was chosen such that the lowest dimensionless wave number for bars was $\lambda = \pi B/L = 0.2$. The numerical domain was discretized using 128 cells along the longitudinal direction, 32 along the transversal, and 50 along the vertical. Periodic boundary conditions were imposed longitudinally. A summary of the runs performed with the values of main parameters is reported in Table 3.

[44] The simulations were started from an initially flat bed, with imposed small-scale disturbances in the form of five longitudinal and five transversal harmonics with different amplitudes in order to trigger the formation of bars. The simulations proceeded until an equilibrium configuration of the bed was reached or bar emersion occurred. Under these conditions, the main characteristics of the bars were calculated, namely bar height, celerity, maximum scour and deposition, and maximum longitudinal and transversal inclinations. As an example, the equilibrium bed configuration of the numerical simulation run 8 achieved employing the NLM, is shown in Figure 14. The displayed pattern is typical of an alternate bar morphology, and is characterized

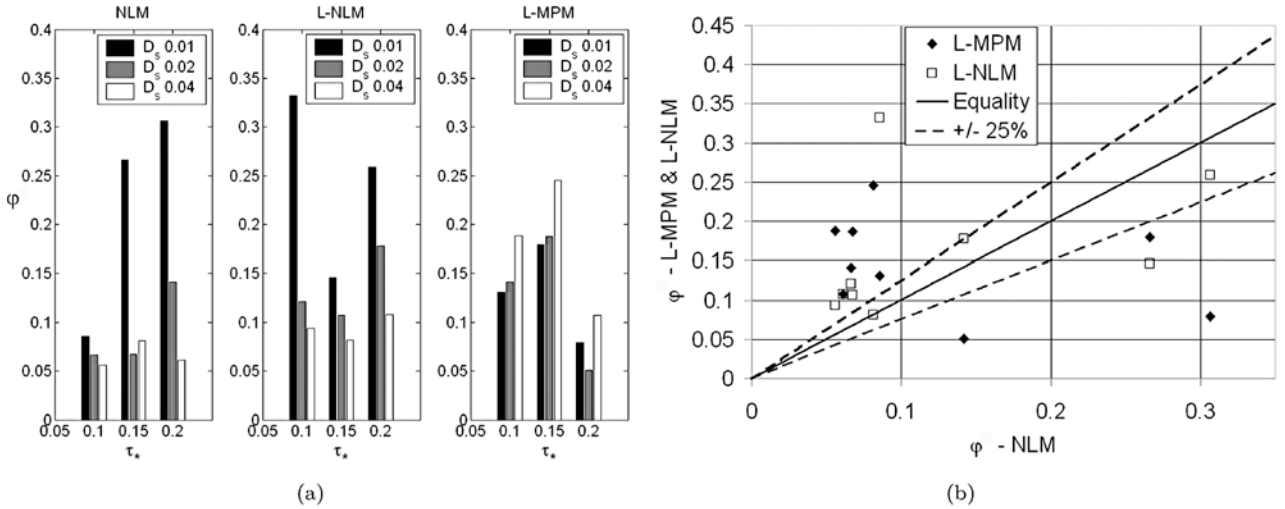

Figure 17. Alternate bars characteristics obtained from numerical simulations using different bed load closures: (a) transversal inclination and (b) comparison of the maximum transversal bed inclination obtained with the linear (vertical axis: L-MPM and L-NLM) and nonlinear (horizontal axis: NLM) formulations.

by a sequence of steep consecutive diagonal fronts with deep pools at the downstream face and gentler riffles along the upstream face.

[45] To better illustrate the role played by the different bed load formulations on the equilibrium bar patterns, in Figures 15–17 the results obtained using the L-MPM and the L-NLM are compared with corresponding quantities obtained with the NLM.

[46] The celerity of migration of the bar pattern, evaluated as the ratio of average space traveled by a bar wave over a time step, is shown in Figure 15. In all the bed load transport closures, bar celerity increased slightly with the applied Shields stress, and also with higher values of D_s (hence with shallower water depth compared to the fixed dimensional sediment size). Comparing the three formulations, it appears that the L-MPM systematically predicted a much larger celerity than the NLM. This finding is, at least qualitatively, in agreement with *Lanzoni* [2000] who found that the experimental celerity of alternate bars was much smaller than the one calculated using a linear bed load formulation. However, note that in the work by *Lanzoni* [2000] the bar celerity was calculated with a linear hydromorphodynamic model, which is strictly valid only for bars at their incipient formation; when the bars grow, nonlinear interactions are likely to influence bar celerity appreciably.

[47] Figure 16 shows a comparison of the maximum longitudinal bed inclination exhibited by the alternate bars. It appears that the NLM and the L-NLM give similar results, while the L-MPM gives on average slightly higher values. The data do not show any appreciable effect of the parameter D_s. In Figure 17 a comparison of the maximum transversal bed inclination is reported. The trend of the data seems to be related to the values of D_s: in the case of D_s = 0.01 the higher values of transversal inclinations are predicted by the NLM, while for D_s = 0.04 the higher values are predicted by the L-MPM. Note that the latter formulation predicts values that are slightly influenced by D_s, while the NLM and L-NLM predict values of transversal inclination that increase with the applied Shields stress and decrease with the parameter D_s. This behavior of the longitudinal and transversal inclinations may be due to the higher values of the intensity of the bed load transport given by the NLM, which renders the bed topography less steep.

6. Conclusions

[48] In the present work the effects of local longitudinal and transversal high slopes on bed load transport is investigated, in order to analyze the gravitational effects on bed load transport and on the dynamics of fluvial bed forms.

[49] Experiments were performed to observe the evolution of a mobile bed from an initial arbitrarily sloping configuration to the final laterally flat equilibrium configuration. In order to evaluate the bed load transport over an arbitrarily sloping bed, the measured bed profiles were compared with the results obtained from a three-dimensional numerical model employing three different closure relationships: (1) the classical bed load transport equation of *Meyer-Peter and Müller* [1948] in the revised form proposed by *Wong and Parker* [2006], coupled with the linear relationship of *Ikeda* [1982] (L-MPM); (2) the nonlinear formulation [*Parker et al.*, 2003] (NLM); and (3) its linearized approximation (L-NLM). Comparison between experimental measurements and numerical results suggests that the morphodynamic evolution is well captured when the nonlinear effects on the bed load are included. In particular, results suggest that the classical linear formulation (L-MPM) leads to a significant underestimation of the lateral bed load transport, which prevents the model from adequately describing the bed evolution.

[50] These findings open important issues on the most reliable closure relationships for sediment transport to be used in morphodynamic studies. We have shown that the inclusion of the nonlinear gravitational effects (i.e., the effects of local high slopes) can affect the dynamics of bed forms like bars by comparing the numerical results obtained using the different formulations for bed load in a straight channel. In fact, results obtained with the nonlinear model are significantly different (especially for the average bar celerity) from those obtained with the linear formulations.

[51] **Acknowledgments.** Gianluca Vignoli is gratefully acknowledged for interesting discussions and suggestions about this work, for providing the numerical code, and for his help. The authors are grateful to Enio Paris, University of Florence (Italy), for scientific comments and his encouragement to develop this work.

References

Abbott, J. E., and J. R. D. Francis (1977), Saltation and suspension trajectories of solid grains in a water streams, *Philos. Trans. R. Soc. London, Ser. A*, *284*, 225–254.

Ashida, K., and M. Michiue (1972), Study on hydraulic resistance and bedload transport rate in alluvial streams, *Trans. Jpn. Soc. Civil Eng.*, *206*, 59–69.

Bagnold, R. A. (1956), The flow of cohesionless grains in fluids, *Philos. Trans. R. Soc. London, Ser. A*, *249*, 235–297.

Bridge, J. S., and S. J. Bennett (1992), A model for the entrainment and transport of sediment grains of mixed sizes, shapes and densities, *Water Resour. Res.*, *28*(2), 337–363.

Casulli, V., and E. Cattani (1994), Stability, accuracy and efficiency of a semi-implicit method for three dimensional shallow flow, *Comput. Math. Appl.*, *27*(1), 99–112.

Colombini, M., G. Seminara, and M. Tubino (1987), Finite-amplitude bars, *J. Fluid Mech.*, *181*, 213–232.

Damgaard, J. S., R. J. S. Whitehouse, and R. L. Soulsby (1997), bedload sediment transport on steep longitudinal slopes, *J. Hydraul. Eng.*, *123*(12), 1130–1138.

Dean, R. B. (1974), Reynolds number dependence on skin friction in two dimensional rectangular duct flow and a discussion on the law of the Wake, *AERO Rep. 74-11*, Imperial Coll., London.

Dey, S. (2003), Threshold of sediment motion on combined transverse and longitudinal sloping beds, *J. Hydraul. Res.*, *41*(4), 405–415.

Engelund, F., and J. Fredsoe (1976), A sediment transport model for straight alluvial channels, *Nord. Hydrol.*, *7*, 293–306.

Fernandez Luque, R., and R. van Beek (1976), Erosion and transport of bedload sediment, *J. Hydraul. Res.*, *14*(2), 127–144.

Francalanci, S., and L. Solari (2007), Gravitational effects on bed load transport at low Shields stress: Experimental observations, *Water Resour. Res.*, *43*, W03424, doi:10.1029/2005WR004715.

Francalanci, S., and L. Solari (2008a), Bedload transport equation on arbitrarily sloping bed, *J. Hydraul. Eng.*, *134*(1), 110–115, doi:10.1061/(ASCE)0733-9429(2008)134:1(110).

Francalanci, S., and L. Solari (2008b), Experimental observations on the motion of bedload particles over an arbitrarily tilted bed, in *Proceedings of the International Conference on River Hydraulics, Cesme-Izmir, Turkey, 3–5 September 2008*, edited by M. A. Altinakar et al., pp. 953–957, Kubaba Congr. Dep. and Travel Serv., Ankara, Turkey.

Francalanci, S., L. Solari, and G. Vignoli (2006), Gravitational effects on river morphodynamics, in *River Flow 2006: Proceedings of the International Conference on Fluvial Hydraulics, Lisbon, Portugal, 6–8 September 2006*, pp. 1129–1136, Taylor and Francis, London.

Francis, J. R. D. (1973), Experiments in the motion of solitary grains along the bed of a water stream, *Proc. R. Soc. London, Ser. A*, *332*, 443–471.

Hu, C., and Y. Hui (1996), Bed-load transport. I: Mechanical characteristics, *J. Hydraul. Eng.*, *122*(5), 245–254.

Ikeda, S. (1982), Lateral bed load transport on side slopes, *J. Hydraul. Div.*, *108*(11), 1369–1373.

Kovacs, A., and G. Parker (1994), A new vectorial bedload formulation and its application to the time evolution of straight river channel, *J. Fluid Mech.*, *267*, 153–183.

Lanzoni, S. (2000), Experiments of bar formation in a straight flume Gravel saltation: 1. Uniform sediments, *Water Resour. Res.*, *36*(11), 3337–3349.

Lee, H. Y., and I. S. Hsu (1994), Investigation of saltating particle motions, *J. Hydraul. Eng.*, *120*(7), 831–845.

Lee, H. Y., Y. H. Chen, J. Y. You, and Y. T. Lin (2000), Investigations of continuous bed load saltating process, *J. Hydraul. Eng.*, *126*(9), 691–700.

Meyer-Peter, E., and R. Müller (1948), Formulas for bed-loaded transport, in *Report on the Second Meeting*, pp. 39–64, Int. Assoc. of Hydraul. Eng. and Res., Madrid.

Nino, Y., and M. Garcia (1994a), Gravel saltation: 1. Experiments, *Water Resour. Res.*, *30*(6), 1907–1914.

Nino, Y., and M. Garcia (1994b), Gravel saltation: 2. Modeling, *Water Resour. Res.*, *30*(6), 1915–1924.

Parker, G. (1984), Lateral bed load transport on side slopes, *J. Hydraul. Div.*, *110*(2), 197–199.

Parker, G., G. Seminara, and L. Solari (2003), Bedload at low shields stress on arbitrarily sloping beds: Alternative entrainment formulation, *Water Resour. Res.*, *39*(7), 1249, doi:10.1029/2001WR000681.

Parker, G., P. R. Wilcock, C. Paola, W. E. Dietrich, and J. Pitlick (2007), Physical basis for quasi-universal relations describing bankfull hydraulic geometry of single-thread gravel bed rivers, *J. Geophys. Res.*, *112*, F04005, doi:10.1029/2006JF000549.

Sekine, M., and M. Kikkaua (1992), Mechanics of saltating grains, *J. Hydraul. Eng.*, *118*(4), 536–558.

Sekine, M., and G. Parker (1992), Bedload transport on transverse slopes, *J. Hydraul. Eng.*, *118*(4), 513–535.

Seminara, G. (1998), Stability and morphodynamics, *Meccanica*, *33*, 59–99.

Seminara, G., L. Solari, and G. Parker (2002), Bed load at low shields stress on arbitrarily sloping beds: Failure of the Bagnold hypothesis, *Water Resour. Res.*, *38*(11), 1183, doi:10.1029/2001WR001253.

Struiksma, N., K. W. Olesen, C. Folkstra, and H. I. De Vriend (1984), Bed deformation in curved alluvial channels, *J. Hydraul. Res.*, *23*, 57–79.

Talmon, A. M., M. C. L. M. Mierlo, and N. Van Struiskma (1995), Laboratory measurements of the direction of sediment transport on transverse alluvial-bed slopes, *J. Hydraul. Res.*, *33*, 495–517.

Toffolon, M., and G. Vignoli (2007), Suspended sediment concentration profiles in nonuniform flows: Is the classical perturbative approach suitable for depth-averaged closures?, *Water Resour. Res.*, *43*, W04432, doi:10.1029/2006WR005183.

Vignoli, G. (2005), *Modelling the Morphodynamics of Tidal Channels*, 129 pp., Univ. of Trento, Trento, Italy. (Available at http://portale.unitn.it/dree/portalpage.do?channelId=-35931)

Vignoli, G., and M. Tubino (2002), A numerical model for sand bar stability, in *Proceedings of the International Conference on Fluvial Hydraulics, River Flow 2002, Louvain-La-Neuve, Belgium, 4–6 September 2002*, vol. 2, edited by D. Bousmar and Y. Zech, pp. 833–841, Swets and Zeitlinger, Lisse, Netherlands.

Wiberg, P. L., and J. D. Smith (1985), A theoretical model for saltating grains in water, *J. Geophys. Res.*, *90*(C4), 7341–7354.

Wiberg, P. L., and J. D. Smith (1989), Model for calculating bedload transport of sediment, *J. Hydraul. Eng.*, *115*(1), 101–123.

Wong, M., and G. Parker (2006), Reanalysis and correction of bedload relation of Meyer-Peter and Müller using their own database, *J. Hydraul. Eng.*, *132*(11), 1159–1168, doi:10.1061/(ASCE)0733-9429(2006)132:11(1159).

S. Francalanci, Center of Research and Advanced Education for Hydrogeological Risk Prevention, Via XI Febbraio 2, I-55040 Retignano, Italy. (simona.francalanci@dicea.unifi.it)

L. Solari, Department of Civil and Environmental Engineering, University of Florence, Via S.Marta 3, I-50139 Florence, Italy. (luca.solari@dicea.unifi.it)

M. Toffolon, Department of Civil and Environmental Engineering, University of Trento, Via Mesiano 77, I-38050 Trento, Italy. (marco.toffolon@ing.unitn.it)